CO_2 and albedo climate impacts of extratropical carbon and biomass plantations

M. Schaeffer,[1,2] B. Eickhout,[1] M. Hoogwijk,[1,3] B. Strengers,[1] D. van Vuuren,[1] R. Leemans,[4] and T. Opsteegh[5]

Received 29 June 2005; revised 9 February 2006; accepted 27 February 2006; published 22 June 2006.

[1] We explored the climate impacts for two land-use change scenarios, aimed at mitigating the buildup of greenhouse gases in the atmosphere. Using the integrated assessment model IMAGE 2.2, we found that the large-scale implementation in the extratropics of either carbon-sequestration or modern-biomass plantations decreases the CO_2 concentration with 70–80 ppmv by the year 2100 compared to a nonmitigation baseline. In a coupled land/atmosphere/ocean/sea-ice model this moderates global warming over the 21st century by 10%. However, the carbon-sequestration option raises the absorption of solar radiation due to a lower albedo compared to the scenario involving modern-biomass plantations (for biofuels production). The albedo-induced difference in global mean temperature is as large as the mitigation by CO_2 changes in the two scenarios compared to the baseline. Further, an atmospheric circulation change in the carbon-plantation scenario weakens the supply of moisture from the oceans to North Africa and central Eurasia. In our model this decreases annual mean precipitation over North Africa by up to 10% and further increases summer temperatures over Eurasia. These findings lead us to conclude that other climate impacts than just CO_2 changes have to be taken into account when discussing climate-change mitigation options that involve land-use changes.

Citation: Schaeffer, M., B. Eickhout, M. Hoogwijk, B. Strengers, D. P. van Vuuren, R. Leemans, and T. Opsteegh (2006), CO_2 and albedo climate impacts of extratropical carbon and biomass plantations, *Global Biogeochem. Cycles*, *20*, GB2020, doi:10.1029/2005GB002581.

1. Introduction

[2] A wide range of options has been proposed to mitigate the buildup of greenhouse gases in the atmosphere, for compliance with Article 2 of the United Nations Framework Convention on Climate Change. These options include improvements to energy efficiency, changes in energy production, measures to reduce emissions of non-CO_2 greenhouse gasses and measures to increase the carbon uptake of sinks. Some of these options could also have considerable consequences for land-use patterns, in particular large-scale production of biofuels (to substitute the use of fossil fuels) and the use of carbon plantations (to enhance CO_2 sequestration).

[3] Modeling studies, well validated with detailed observations, show that changing land use in the past centuries influenced local, regional and likely also global climate patterns [e.g., *Chase et al.*, 2000; *Intergovernmental Panel on Climate Change* (*IPCC*), 2001; *Pielke et al.*, 2002]. Historically, land-use mediated climate change appears to be an important factor [*Brovkin et al.*, 1999]. In mid to high latitudes, for example, land-use changes influence surface-air temperature, because of the large difference in surface albedo between different land covers, such as cropland and forest in snow-covered conditions [*Robinson and Kukla*, 1985; *Bonan et al.*, 1995; *Harding and Pomeroy*, 1996; *Sharrat*, 1998]. This implies that the mitigation options that affect (future) land cover might not only influence climate change by reducing global greenhouse-gas concentrations, but also have an impact on the energy fluxes between land surface and the atmosphere [*Betts*, 2000; *Pielke*, 2001a; *Pielke et al.*, 2002; *Marland et al.*, 2003]. *Betts* [2000] estimated the effect of coniferous carbon plantations in the Northern Hemisphere on planetary albedo. His calculations suggest that the warming by albedo changes associated with high-latitude forestation would outweigh global cooling by carbon sequestration.

[4] The analysis of *Betts* [2000] was performed as a sensitivity analysis under extreme assumptions: All forest and agricultural regions were transformed to carbon plantations, irrespective of demand for other land uses, like food and fodder. Additionally, only a rough indication of local

[1]Netherlands Environmental Assessment Agency (MNP-RIVM), Bilthoven, Netherlands.
[2]Now at Wageningen University, Wageningen, Netherlands.
[3]Now at Ecofys B.V., Utrecht, Netherlands.
[4]Environmental Systems Analysis Group, Wageningen University, Wageningen, Netherlands.
[5]Institute for Marine and Atmospheric Research, Faculty of Physics and Astronomy, Utrecht University, Utrecht, Netherlands.

0886-6236/06/2005GB002581$12.00

carbon sequestration potential was used. Given the importance of the albedo impacts found by *Betts* [2000], it seems worthwhile to further explore the climate consequences of mitigation options that alter land use patterns significantly. In this study, we will compare biomass and carbon plantations, taking into account both the effects on the carbon cycle (''biogeochemical impact'') and on energy fluxes (''biophysical impact'') for the period 2000–2100. We will focus on the effect of albedo changes as in the work of *Betts* [2000], since this is a relatively robust feature of the physical influence of land cover change on climate at mid to high latitudes.

[5] The use of modern biomass from energy plantations has been proposed to (partly) substitute fossil fuels, in particular in the transport sector and for electricity generation. A large number of crops or trees could be used to produce the primary biomass feedstocks, which can be converted into secondary energy carriers. For temperate zones, attractive biomass sources include woody biomass (e.g., willow and poplar), maize, seeds and sugar beets. The energy-supply potential of modern biomass plantations (henceforth MB plantations) has been assessed in a number of papers. The technical potential has been estimated to reach a maximum of between 10% and more than 100% of total global primary energy consumption by 2100, depending on assumptions on technological change in food and energy crop production systems, competition with other types of land use and the strictness of climate policies [*Berndes et al.*, 2003; *Hoogwijk et al.*, 2005].

[6] A second option is the large-scale application of carbon plantations (C plantations) that consist of vegetation types selected to provide an optimal net CO_2 uptake under local climate conditions. Active afforestation policies and forest management can enhance carbon uptake compared to natural systems. Without harvesting, the net gain in uptake could typically last several decades; in combination with harvesting, the net gain will continue assuming the harvested wood is used to displace fossil fuels as biofuel and/or wood from natural forests as timber. In the extratropical Northern Hemisphere (NH), the appropriate species is often coniferous trees [*Nabuurs and Mohren*, 1996].

[7] Our analysis starts by applying our integrated assessment model IMAGE 2 [*Alcamo et al.*, 1998] to develop a scenario projection of future abandoned agricultural land. This provides a more realistic estimate of the geographical potential for carbon and modern-biomass plantations compared to *Betts* [2000]. IMAGE 2 has been used for a wide range of scientific and policy-advice studies, including a major contribution to the IPCC SRES scenarios [*IPCC*, 2000; *IMAGE-team*, 2001a], a study on the importance of different feedback processes [*Leemans et al.*, 2002], the exploration of the geographical carbon sequestration potential of C plantations (J. G. van Minnen et al., The role of carbon plantations in mitigating climate change: Methodology and first results, manuscript in preparation, 2006) (hereinafter referred to as van Minnen et al., manuscript in preparation, 2006) and estimates of the geographical potential for modern biomass [*Hoogwijk et al.*, 2005]. This paper combines the isolated results of these studies and provides a more comprehensive analysis. Moreover, IMAGE-2 will be combined with ECBilt-CLIO, an atmosphere/ocean general circulation model of intermediate complexity, which was used extensively in studies of climate variability and change [*Opsteegh et al.*, 1998; *Schaeffer et al.*, 2002]. This model will complete the evaluation by allowing the assessment of the climate impacts of the associated changes in albedo in addition to the CO_2 changes.

[8] In section 2, we will build on the previous IMAGE-2.2 work as mentioned above to develop a set of scenarios for future large-scale application of modern-biomass and carbon plantations. In section 3, we will describe relevant features of the models and outline the experiments. ECBilt-CLIO output is compared to observations in section 4, focusing on the performance of a new albedo parameterization in the model. The results of the experiments are analyzed in section 5 (impact on carbon fluxes), 6 (changes in surface albedo) and 7 (climate impacts). A short discussion in section 8 concludes the paper.

2. Scenarios and Assumptions

2.1. Scenario Development

[9] In this study we use the IMAGE implementation of the scenarios in the IPCC SRES (Special Report on Emission Scenarios [*IPCC*, 2000; *IMAGE-team*, 2001a]). The IPCC SRES scenarios were developed by several modeling teams to explore the different possible pathways regarding greenhouse-gas emissions in the 21st century, and include consistent trajectories of human activities (i.e., the so-called ''drivers''). Two teams (IMAGE and AIM) elaborated on the SRES storylines also in terms of geographically explicit land-use scenarios [*Strengers et al.*, 2004]. This work showed that for two out of the four scenario families (A1 and B1) large areas of agricultural land might be abandoned in the course of the 21st century as a result of further increases in agricultural yields, and a stabilizing and even declining global population. In this study the carbon and modern-biomass plantation experiments are based on the A1b scenario, which combines strong globalization and international governance with economic development policies (the latter as opposed to social and environmental objectives).

2.2. Geographic Potential for Carbon and Modern-Biomass Plantations

[10] In the literature, the use of carbon (C) and modern-biomass (MB) plantations is considered both on more degraded, or marginal, lands and on productive (often abandoned agricultural) land. As the first uses low productive lands, production will mostly be extensive. Here we concentrate on the productive grounds. In agreement with most studies, we also assume that C and MB plantations will mainly take place on areas not used for the production of food, fodder and forestry products. Moreover, we assume that areas that are currently forests will not be converted to either MB, or C plantations (for example because of conservation policies) (van Minnen et al., manuscript in preparation, 2006).

[11] The assumptions above imply that in temperate zones excess agricultural areas could provide the most interesting locations for either MB, or C plantations. The time-dependent geographically explicit scenario for the potential future application of MB and C-plantations in this paper is based on the IPCC A1b scenario of *Hoogwijk et al.* [2005]. In this scenario, agricultural land is abandoned because of a surplus of agricultural area, or a shift toward more productive sites (driven by climate change).

[12] Please note that the scenario experiments in this paper are illustrative and assume extreme situations in order to investigate the potential impact of the surface-albedo changes. These sensitivity experiments differ from other long-term land-use scenarios using the IMAGE-2.2 model in which demand for land has been matched with resources of land, resulting in a more plausible future trend.

3. Description of Models and Further Specification of Sensitivity Experiments

3.1. IMAGE-2.2 Model and Experiment Setup

[13] The general objective of IMAGE 2.2 is to explore the long-term dynamics of global environmental change. The model consists of several linked modules [*Alcamo et al.*, 1998; *IMAGE-team*, 2001a]. The main driving forces are economic and demographic trends at a regional level. Energy system drivers (production and consumption flows) are simulated in TIMER together with related emissions of GHGs (GreenHouse Gases) and regional air pollutants (Targets IMage Energy Regional model [*de Vries et al.*, 2001]). Ecosystem, crop and land-use modules are used to compute land use on the basis of regional consumption, production and trading of food, animal feed, fodder, grass and timber, and local climatic and soil properties. The exchange of CO_2 between terrestrial ecosystems and the atmosphere is simulated [*Leemans et al.*, 2002; *Strengers et al.*, 2004]. The atmospheric and ocean models calculate changes in atmospheric composition by employing the emissions and by taking oceanic CO_2 uptake and atmospheric chemistry into consideration. Subsequently, changes in climatic properties are computed [*Eickhout et al.*, 2004]. Changes in climate and CO_2 concentration are feeding back on the land-cover projections. Of special interest for the present paper are the characteristics of TIMER and the terrestrial modules, the latter functioning on a $0.5^\circ \times 0.5^\circ$ grid.

3.2. IMAGE Energy Model TIMER

[14] In this paper, the TIMER 1.0 energy model is used to assess the potential impact of increased use of biofuel on fossil-fuel greenhouse gas emissions (for details see *de Vries et al.* [2001] and *van Vuuren et al.* [2006]). TIMER describes the energy consumption and production for 10 primary energy carriers for which market shares are determined on the basis of assumed consumer preferences and costs. In the model, biofuels mainly compete in the transport sector (with oil-based alternatives) and in the electric power sector (offsetting natural gas and coal use). Under the IMAGE-A1b scenario, biofuels reach a production level of about 250 EJ worldwide in 2100, i.e., around 15% of global primary energy consumption. For the purpose of this analysis, however, we have defined the use of biofuels exogenously. We applied a set of simple assumptions to determine how biofuels will be used.

[15] 1. In the "no-biofuel" variant, the production of biofuels in NH regions has been set to zero. The supply of biofuels in all regions is reduced through the impact of this reduction on global biofuel supply. As a result, the market shares for biofuels are replaced by fossil-fuel based alternatives, mostly oil and natural gas.

[16] 2. In the "exogenous-biofuel" variant, the supply of biofuel in NH regions is set exogenously to the maximum potential as identified by *Hoogwijk et al.* [2005]. TIMER uses an efficiency of 40–60% to convert primary energy carriers such as biomass to electricity. In the transport sector, TIMER only uses secondary biomass fuels. As *Hoogwijk et al.* [2005] give total primary energy numbers for biofuels, we had to partly convert these numbers. On the basis of the assumption that 50% of the biofuels will be used in transport using a conversion efficiency from primary biomass to transport fuel, the primary energy production numbers have been multiplied by 0.7. For simplification, we assumed that the increased biomass supply will equally increase biomass use in all regions globally, and across all sectors. In the transport sector, the additional biomass is assumed to substitute oil use. In the electricity sector, it is assumed that biomass will substitute natural gas use (a more conservative estimate compared to coal; moreover, natural gas has the largest market share in new electric power capacity in this scenario). Indirectly, some further changes may occur as the additional biomass affects the prices of fossil fuels.

[17] In both cases, the impact on emissions is calculated, with noticeable changes for greenhouse gas emissions and sulphur emissions.

3.3. IMAGE Terrestrial Models

[18] Land-cover transformations are driven by a complex interplay of social, physical and economic forces. These processes are integrated in IMAGE 2.2 in a simplified manner by heuristic land-use rules. The terrestrial models distinguish four land cover transitions: (1) natural vegetation to agricultural land (either cropland or pasture) because of the need for additional agricultural land; (2) agricultural land to other land cover types because of the abandonment or unsuitability (under climate change) of agricultural land; (3) forests to "regrowth forests" because of timber and fuelwood extraction; and (4) one type of natural vegetation to another because of climate change and/or change in water use efficiency. The land-cover model allocates the agricultural demand (including wood demand) grid cell by grid cell within each region, giving preference to cells with the highest probability for satisfying this demand [*Alcamo et al.*, 1998]. Crops are assigned to agricultural cells according to their crop productivity. The crop productivity is based on climate circumstances, soil characteristics and the CO_2 concentration [*Leemans and van den Born*, 1994]. A central assumption is that agricultural high-yield areas and areas close to established infrastructure are preferable locations to retain food- and fodder-growing purposes.

Table 1a. Representative Tree Species Selected for Carbon Plantations in IMAGE and Their Climatic Characteristics[a]

Number	Tree Species	Corresponding PFT	T_{cold} (°C)	Moisture	$GDD5_{min}$
1	*Eucalyptus camadulensis*	tropical deciduous	>15.5	0.45 to 0.8	
2	*Eucalyptus grandis*	tropical evergreen	>15.5	>0.8	
3	*Pinus radiata*	temperate evergreen	>5	0.55 to 0.95	
4	*Populus nigra*	temperate deciduous	−15 to 15.5	>0.65	>1200
5	*Picea abies*	boreal evergreen	−35 to −2	>0.75	>350
6	*Larix kaempferi*	boreal deciduous	<5	>0.65	>350

[a]T_{cold}, the average temperature of the coldest month; Moisture, annual moisture index expressed as the Priestley Taylor index [*Cramer and Solomon*, 1993], i.e., the actual evapotranspiration divided by the potential evapotranspiration (the lower end of the range can decline due to increasing water use efficiency (WUE), a result of increasing atmospheric CO_2 levels); $GDD5_{min}$, the minimum degree-day sum for establishment (considering a 5°C base).

[19] In the normal mode, abandoned agricultural land is transformed to natural vegetation as determined by the natural vegetation model (a modified version of the BIOME-model [*Prentice et al.*, 1992]) on the basis of the climate conditions and the CO_2 concentration level. Changes in atmospheric CO_2 concentrations, climate and the effects of land-use and land-cover change are also considered. Calibration has led to an improved simulation of historical land cover and carbon fluxes [*Leemans et al.*, 2002].

[20] When abandoned agricultural land is covered completely by MB plantations (in our case ''woody biofuels'' like eucalyptus, willow and poplar), the carbon uptake is simulated consistently with the crop productivity that was used as input for the biomass energy potential (see above and *Hoogwijk et al.* [2005]). The high carbon uptake of MB plantations is partly offset by higher soil respiration fluxes, mainly the result of decomposing organic material after crop rotation.

[21] In the case of C plantations, the model selects the most suitable tree type out of six representative types on the basis of climate constraints and the highest calculated average net primary production (NPP) of the different types under climate and soil conditions of the grid cell in question. The additional carbon sequestration of C plantations, compared to natural vegetation types, is implemented in the carbon model on the basis of a literature survey (see Tables 1a and 1b for the additional C-cycle parameters taken from van Minnen et al. (manuscript in preparation, 2006)).

3.4. The Three Land-Use Change Experiments With IMAGE

[22] Three modified versions of the A1b scenario for the period 2000–2100 have been used as input for the experiments (Table 2). In the first experiment, no demand for biofuels in the NH extratropical regions is assumed (IM-nat). All former agricultural land returns to vegetation types given by the natural vegetation model. This forms the nonmitigation ''baseline scenario'' used as a benchmark to compare the effectiveness of the two plantation mitigation options.

[23] In the second experiment, IM-C, all abandoned cropland will be used for C plantations and the land-atmosphere CO_2 fluxes are modified accordingly. For the energy sector there will be no difference with the IM-nat experiment. In IM-C the abandoned land is only transformed into C plantations when the NPP of these plantations is substantially (more than 1 tC ha^{-1} yr^{-1}) higher compared with the natural regrowing vegetation (somewhat limiting the area of abandoned agricultural land converted to C plantations).

[24] In the third experiment, IM-bio, all abandoned cropland will be used for MB plantations. For this scenario, the exogenous-biofuel variant of IMAGE-TIMER (see above) is used on the basis of the technical potential of this abandoned area (in accordance with *Hoogwijk et al.* [2005]). Part of the resulting reduction in emissions in the energy sector is offset by an additional amount of carbon emitted through burning of the aboveground biomass harvest.

[25] In Figure 1, the different land-use change scenarios are visualized. Because we assume that biomass crops are planted on all abandoned cropland, the total area of MB plantations is larger than of C plantations in the IM-C experiment with the additional ''NPP constraint.'' In Figure 2, the areas of plantations over time are given for the distinguished regions, showing that in all regions the largest area increase occurs in the first half of the 21st

Table 1b. Representative Tree Species Selected for Carbon Plantations in IMAGE and Their Carbon Characteristics[a]

Number	Corresponding LCT	Yield, m^3/ha/yr	Recov, years	LRP, years	HI	WD, tdm/m^3	NPP_{max}, TC/ha/yr
1	tropical deciduous forest	12	8	15	.65	.66	17.1
2	tropical evergreen forest	20	8	15	.70	.50	20.2
3	warm mixed forest	14	15	28	.87	.45	12.4
4	temperate deciduous forest	16	18	25	.83	.35	12.4
5	cool mixed forest	12	30	60	.87	.40	10.7
6	boreal forest	7	25	60	.87	.49	7.3

[a]LCT, land-cover type; Recov, recovery time or the number of years it takes before the canopy is closed and the net primary production of the carbon plantation has reached the value NPP_{max} (last column); LRP, the likely rotation period; HI, the harvest index; WD, the wood density of the tree species considered in ton dry matter per cubic meter fresh volume; NPP_{max}, the average net primary production of a carbon plantation after its recovery time: It has been computed by combining different yield tables, recovery times, likely rotation periods (LRP), harvest indices (HI), and wood densities (WD) from literature (see also van Minnen et al., manuscript in preparation, 2006).

Table 2. Summary of Adapted IPCC-A1b Model Experiments

Experiment Name	Model Name	Short Description
IM-nat	IMAGE 2.2	abandoned agricultural land becomes natural vegetation, no exogenous biofuels in TIMER
IM-C	IMAGE 2.2	abandoned agricultural land becomes C plantation, no exogenous biofuels in TIMER
IM-bio	IMAGE 2.2	abandoned agricultural land becomes MB plantation
EC-nat-GHG	ECBilt-CLIO	GHG pathway from IM-nat
EC-nat-TOT	ECBilt-CLIO	GHG and land-cover change from IM-nat
EC-C-GHG	ECBilt-CLIO	GHG pathway from IM-C
EC-C-TOT	ECBilt-CLIO	GHG and land-cover change from IM-C
EC-bio-GHG	ECBilt-CLIO	GHG pathway from IM-bio
EC-bio-TOT	ECBilt-CLIO	GHG and land-cover change from IM-bio

century, except in China. By the year 2100, an area of about 800 Mha is converted to plantations in the IM-C experiment, against more than 950 Mha in the IM-bio experiment.

3.5. ECBilt-CLIO Model and Experiment Setup

[26] For exploring the climate impacts of the IMAGE-2.2 experiments, and thus the effectiveness of the two climate-change mitigation options, we will use the coupled atmosphere/ocean/cryosphere model ECBilt-CLIO. The atmospheric component ECBilt [*Opsteegh et al.*, 1998] was developed for research on the relative importance of the physical feedbacks in the extratropics of the climate system on decadal and longer timescales. Since the main application of this model is in the extratropics, a quasi-geostrophic approach for the dynamical core of the model was adopted. The neglected ageostrophic terms in the vorticity and thermodynamic equations are included as a time and space varying forcing of the geostrophic tendencies. In the extratropics, the performance of the model is comparable to that of general circulation models of similar spatial resolution. The resolution of ECBilt is about 5.6° lat/lon (T21), with three vertical levels. The ocean model CLIO is a general circulation model (GCM) with a dynamic sea-ice component and a relatively sophisticated parameterization of vertical mixing [*Goosse and Fichefet*, 1999]. The horizontal resolution of CLIO is 3 degrees in latitude and longitude, and there are 20 unevenly spaced vertical levels in the ocean. The coupled model (ECBilt-CLIO) was recently used to study the influence of mid- to high latitude atmosphere/ocean/sea-ice interactions on climate variability and change [*Goosse et al.*, 2001; *Renssen et al.*, 2001; *Goosse et al.*, 2002; *Schaeffer et al.*, 2002, 2004, 2005]. The present-day climatology is explored in more detail by *Goosse et al.* [2001]. The estimated global climate sensitivity is 1.7°C for a doubling of CO_2, which is on the low end of the estimated range [*Kattenberg et al.*, 1996; *Gregory et al.*, 2002].

[27] Physical parameterizations in ECBilt were kept as simple as possible. A bucket model of uniform depth (15 cm) represents soil moisture. The land cells are assigned to the world's major river catchment areas and excess soil moisture (runoff) is discharged in the appropriate ocean cells, without time lags. Probably the most important surface/atmosphere energy feedback in the mid to high latitudes is the albedo-snow feedback. In the updated snow model in ECBilt, the snow-layer depth (d, in mm liquid water) is used to determine the albedo α_d. This albedo is

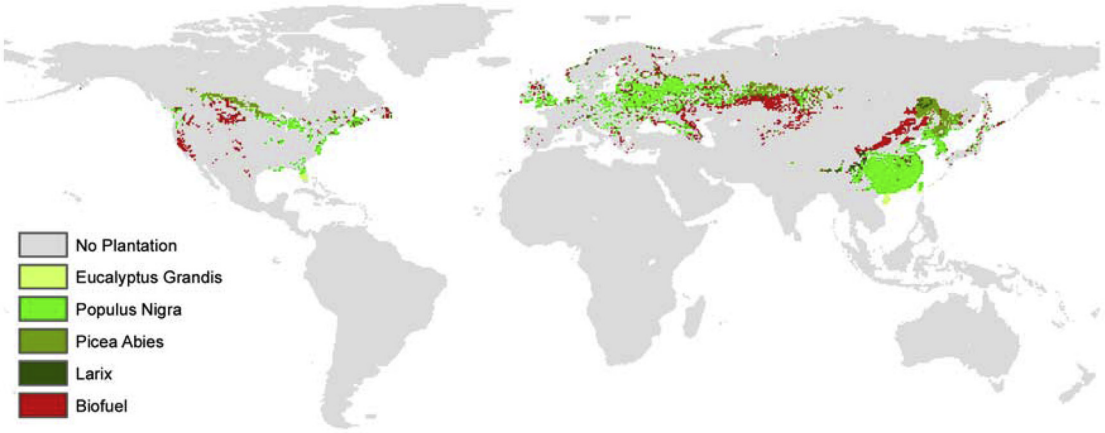

Figure 1. C-plantation tree types for the year 2100 in the IM-C experiment. Because of the extra surplus-NPP constraint on C plantations and bioclimatic limits, the total area of these is smaller than that of MB plantations. The additional area of MB plantations in the IM-bio experiment is indicated in red. Land-cover changes for regions other than the Northern Hemisphere regions selected for the sensitivity experiments in this paper are not shown here.

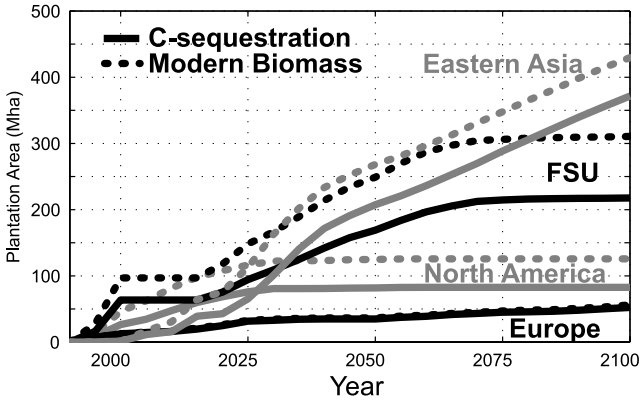

Figure 2. Areas of plantations for the distinguished regions for both the C-sequestration (IM-C) and Modern Biomass (IM-bio) scenarios.

determined by the interpolation between snow-free (α) and completely snow-covered (α_a) albedo:

$$\alpha_d = \alpha + (\alpha_a - \alpha) \cdot \left(1 - e^{-0.2 \cdot d}\right).$$

The snow-covered albedo varies per vegetation type, as in the algorithm of the HadAM3 GCM (see Table 3) [*Cox et al.*, 1999]. In addition, the snow albedo decreases through snow aging [*Hansen et al.*, 1983; *Robinson and Kukla*, 1984],

$$\alpha_a = \alpha_{old} + \left(\alpha_{fresh} - \alpha_{old}\right) \cdot e^{-a/5}.$$

Here α_{fresh} is the maximum fresh-snow albedo, specified for each land-cover type to include snow-masking (see Table 3). Further, a is the snow age in days, reset to zero when snowfall exceeds 1 mm liquid water per hour and α_{old} is the old-snow albedo, calculated as

$$\alpha_{old} = \min\left(\alpha_{fresh}, 0.5\right).$$

[28] In the scenario experiments, the albedo of the grid-cells of ECBilt-CLIO is determined by using land-cover classes from the higher resolution IMAGE-2.2 maps and area weighting the albedo values (see Table 3 and Appendix A). The albedo values are in line with the values used by *Cox et al.* [1999] and *Betts* [2000] and agree with a large range of observations, for which references are indicated in Appendix A. For MB plantations, we have adopted albedo values of deciduous shrubs. However, MB plantations are subject to rotation and snow masking will be "reset" after each harvest. Thus the long-time mean snow-masking effect is smaller than that of undisturbed (natural) mature land cover of the same vegetation type. For MB plantations, we presume that albedo parameters of agricultural land apply in the harvest year and that full snow-masking (using albedo values for deciduous shrubs) is approached with a relaxation (e-folding) time of 1 year for a plantation with rotation period of 5 years. From this, an effective long-time mean albedo is calculated. For C plantations, we assumed that full snow-masking is reached after about 20 years and we have calculated mean albedo over a time horizon of 100 years (no rotation) over which C plantations approach albedo's for evergreen needleleaf, or deciduous broadleaf trees where appropriate. For other land cover types we have neglected a change of albedo parameters associated with the growth of vegetation in time.

[29] Observations by *Robinson and Kukla* [1984] show that in the winter season, snow-free albedo of nonwoody land-cover types is higher than in summer, while the reverse holds for deciduous woody types. This is reflected in the model by raising, or lowering, snow-free albedo in winter and summer accordingly with 0.01 as compared to the annual mean in Table 3 for all nonwoody land-cover types, as well as land-cover types with a major deciduous-vegetation component.

[30] All ECBilt-CLIO experiments start by using initial conditions from a single model spin-up forced by historical GHG concentrations from the years 1850 to 1970. Before this spin-up, the model was brought into equilibrium by running 1000 years with constant 1850 GHG concentrations. For each of the three modified IMAGE-2.2 A1b experiments, we have run ECBilt-CLIO two times: with GHG changes only and with both GHG and land-cover changes (see Table 2).

[31] Since we expected that the difference in climate impact between the scenarios is small, all experiments were performed in ensemble mode, by applying tiny random distortions to the atmospheric initial conditions. Each of 20 individual simulations within one ensemble represents a different evolution of the climate system for the same external forcing, with equal probability of occurrence. The spread in the results among the individual ensemble members thus provides an indication of the influence of internal,

Table 3. Albedo Parameters for IMAGE-2.2 Land-Cover Types[a]

Land-Cover Type	α	α_{fresh}
Agricultural land	0.19	0.75
Modern Biomass plantation	0.18	0.70
C plantation (dense dec. broadleaf forest)	0.14	0.33
C plantation (dense evergr. coniferous forest)	0.12	0.24
Polar desert	0.80	0.80
Polar desert2 (Greenland ice sheet)	0.84	0.84
Polar desert3 (Antarctic ice sheet)	0.87	0.87
Tundra	0.16	0.76
Wooded tundra	0.15	0.62
Boreal forest	0.13	0.41
Cool conifer forest	0.13	0.33
Temperate mixed forest	0.13	0.34
Temperate deciduous forest	0.14	0.37
Warm mixed forest	0.14	0.31
Grassland/steppe (cool grassland)	0.19	0.65
Grassland/steppe (warm grassland)	0.19	0.64
Grassland/steppe (C4 grassland)	0.21	0.61
Sand desert (Sahara)	0.34	-
Sand desert (non-Sahara)	0.27	0.70
Scrubland	0.19	0.61
Savanna	0.18	-
Tropical woodland	0.16	-
Tropical forest	0.13	-

[a]The albedo values are calculated from the tables in Appendix A.

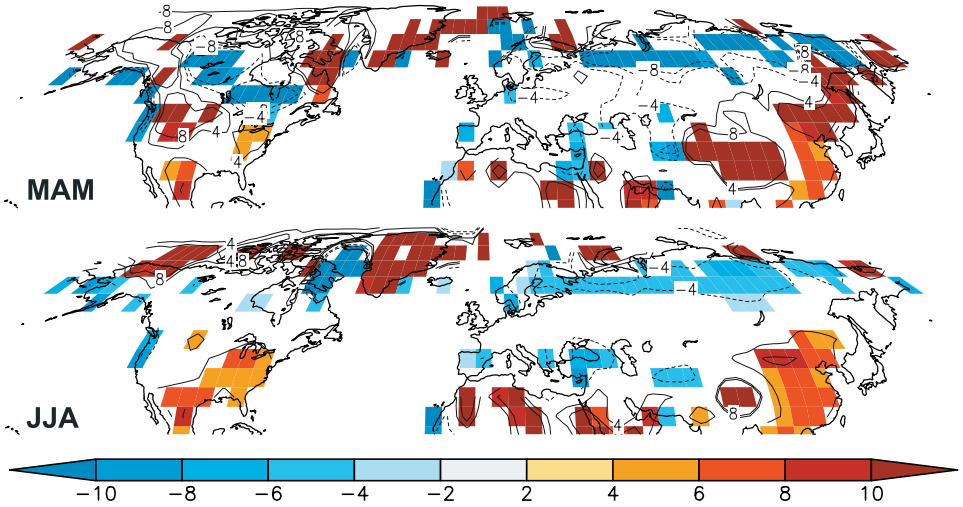

Figure 3. Difference between simulated surface albedo (%) in ECBilt-CLIO and ERBE satellite data averaged over 1986–1989 for (top) March-April-May mean and (bottom) June-July-August mean. Contours are plotted for all model grid cells. Colored are the grid cells for which the difference between the two data sets is significant above the 95% level (see text).

or natural, climate variability on climate change projections. Compared to a single climate model run, the ensemble mean provides a better estimate of the climate response to the forcing, because the influence of internal variability is strongly reduced.

4. Climate Model Validation: Comparison of Albedo Simulations With Observations

[32] Given the importance of albedo effects in this paper, we show, in Figure 3, the surface albedo for the years 1986–1989 in ECBilt-CLIO (mean over all ensembles) using the new snow-albedo parameterization, compared with clear-sky ERBE satellite observations [*Barkstrom*, 1984]. We defined the difference between the two data sets as significant at the 95% level when the mean ERBE albedo deviated from the ECBilt-CLIO mean at least two modeled standard deviations. Note that modeled albedo is a function of the snow-layer climatology in ECBilt and the snow-free and snow-covered albedos assigned to each land-cover type, but also of the IMAGE present-day land-cover map. We focus on the NH spring and summer seasons, in which the difference of albedo between different land-cover types is most influential in terms of radiative forcing. In NH spring (MAM) a large part of the NH is covered with snow. Thus (snow-) albedo differences between land-cover types are large and the influence on climate is stronger than in winter, because of higher insolation. In the NH summer season (JJA) the albedo differences are smaller (snow-free), but insolation is at its peak.

[33] In spring, the modeled albedo is too high where the modeled snow line (not shown) is located farther south than observed [*Foster and Davy*, 1988]. This is the case in northeast China and northwest United States. In west Russia, albedo is underestimated, although snow depth is well simulated. This indicates that the albedo of snow-covered agricultural land is too low here, either because of fresh-snow albedo being too low, or of overestimating the effect of snow aging. Snow-free albedo in this area compares well with the observations. By contrast, the snow-free albedo over agricultural areas in east China and southeast North America is overestimated by a few percent. This indicates that the suitability of a globally uniform value for snow-free albedo of agricultural land is limited.

5. CO_2 Impacts of Plantations

[34] In the no-biofuels variants (IM-nat and IM-C), the use of modern biomass in 2100 is reduced from 250 EJ to 150 EJ per year compared to the original A1b scenario (i.e., only from the tropical NH and the Southern Hemisphere). This increases CO_2 emissions with about 1.6 GtC per year. In the IM-bio case, the worldwide use of modern biomass is increased to 440 EJ yr^{-1} (of which 290 EJ yr^{-1} from NH). As a result, oil use is reduced considerably (by

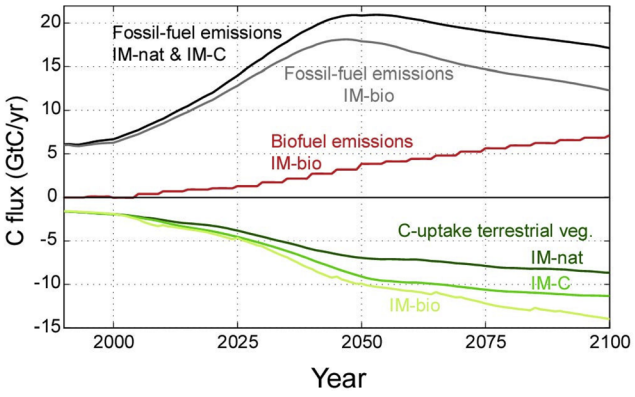

Figure 4. Anthropogenic and terrestrial carbon fluxes for the three land-use experiments.

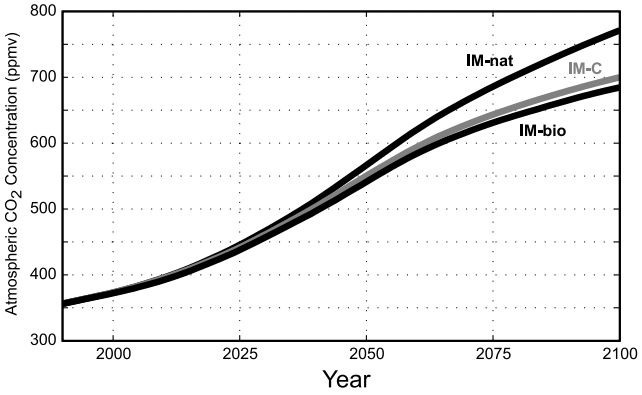

Figure 5. Atmospheric CO_2 concentration in the three land-use experiments.

140 EJ yr^{-1} in 2100). Smaller reductions occur for natural gas (65 EJ yr^{-1}), coal and nuclear/solar/wind.

[35] CO_2 emissions from fossil fuels are reduced from 17 GtC yr^{-1} in 2100 for the IM-nat and IM-C cases to 12 GtC yr^{-1} for IM-bio (see Figure 4). Because of harvesting and burning of biofuels from MB plantations, the gross emission flux from biofuels in IM-bio reaches a level of 7 GtC per year in 2100 (Figure 4). This emission flux more than offsets the gain of using biofuels in the energy sector (5 GtC per year in 2100). This result is in line with the assumption that the burning of biofuels occurs less efficiently than the burning of gas or oil. We assume a heating value of woody biomass of 15 GJ ton^{-1}, while the conversion efficiency in electricity production is 40% in 2000 and increases to 56% in 2050 as a result of technological change.

[36] Figure 4 also shows the terrestrial uptake fluxes of the three different experiments. The terrestrial uptake is highest in the IM-bio case. In this case the plantations are harvested each 5 years, implying a steep carbon uptake curve at the beginning of each new rotation period for these fast-growing crops. Logically, the IM-nat case returns the lowest terrestrial uptake of carbon, since no management is applied to the abandoned agricultural land and the vegetation types are not primarily selected on the basis of optimal carbon sequestration. In the case of IM-C, the terrestrial uptake is higher than IM-nat, benefiting from management of C plantations, but lower than IM-bio, since we assumed no harvest of the C plantations. Note that including rotation in the C-plantation experiment would enhance CO_2 uptake [*Strengers et al.*, 2005; van Minnen et al., manuscript in preparation, 2006]. Since in our experiments the plantation area is very large, including rotation for C plantations requires a very significant change in timber or biomass supplies that we have not implemented.

[37] The consequences for the atmospheric CO_2 concentrations are depicted in Figure 5. The differences between IM-C and IM-bio for the complete carbon cycle can be neglected in light of the uncertainties involved in the carbon budget calculations. As mitigating options, the two mitigation experiments result in a comparable reduction of 70–80 ppmv CO_2 by the year 2100 compared to the non-mitigation experiment IM-nat.

6. Albedo Impacts of Plantations

[38] In the next sections, we will focus on the impact of land-cover changes and CO_2 concentration in the ECBilt-CLIO climate model. Under our assumptions, the short rotation period of the MB plantations (5 years) effectively means that current agricultural land will remain in production. In contrast, this agricultural land is replaced by dense forest in the C plantation, and by natural vegetation in the no-plantation case. Forested areas have a lower albedo than agricultural areas, especially at mid to high latitudes in winter owing to snow-masking [*Robinson and Kukla*, 1985; *Bonan et al.*, 1995; *Harding and Pomeroy*, 1996; *Sharrat*, 1998]. Figure 6 shows that the no-plantation (EC-nat-TOT) and C-plantation (EC-C-TOT) experiments result in a lower global-mean surface albedo than the MB-plantation case (EC-bio-TOT). In all experiments, global warming gradually reduces the snow cover, so that a gradual decline in surface albedo is superimposed on the trends related to land-use change alone. Thus albedo does also decrease somewhat in EC-bio-TOT, as well as in the CO_2-only experiments (not shown). Comparing the two mitigation options, the largest differences are found over the areas of the plantations and the difference in spring is much larger than in summer, because of the remaining snow layer (Figure 7).

7. Climate Impacts

[39] The increase in CO_2 concentration to 770 ppmv in the IM-nat experiment of IPCC SRES A1b leads to a rise in global-mean surface-air temperature (SAT) of 0.8°C by the year 2100 with respect to the 1971–2000 average (Figure 8). This is relatively modest compared to other climate models, because of the low climate sensitivity of

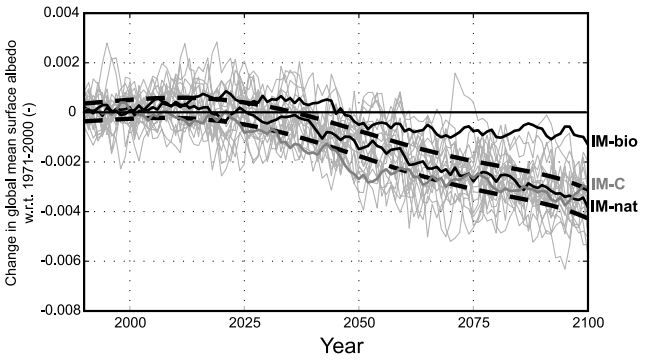

Figure 6. Global and annual mean surface albedo in ECBilt-CLIO with respect to 1971–2000. Thin gray lines are individual ensemble members of the no-plantation baseline experiment. Thick lines are ensemble means of the no-plantation baseline (IM-nat, experiment EC-nat-TOT), C-plantation (IM-C, experiment EC-C-TOT), and MB-plantation (IM-Bio, experiment EC-bio-TOT) experiments. The dashed lines indicate the distance to the baseline case beyond which ensemble means differ from the baseline with 95% significance.

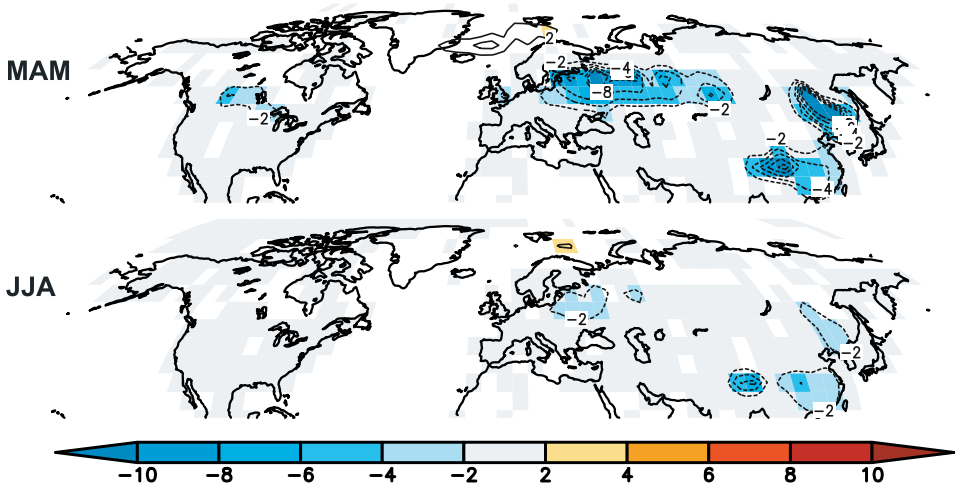

Figure 7. Surface albedo (%) difference of C-plantation (EC-C-TOT) with respect to MB-plantation (EC-bio-TOT) ensemble mean (2071–2100) averaged over (top) March-April-May and (bottom) June-July August. Contours are plotted for all model grid cells. Coloring denotes grid cells for which the difference between the two ensemble means is significant above the 95% level (two-tailed Student's t-test).

ECBilt-CLIO (see section 3). Note also that we have not included the global warming contribution of the 21st century decline in sulphur emissions that is projected in SRES A1b.

[40] By the year 2050, the reduction in CO_2 concentrations causes global-mean SAT in the EC-C-GHG and EC-bio-GHG to diverge from the EC-nat-GHG baseline significantly at the 95% level (1-tailed Student's t-test). Note that the significance level is given by internal climate variability alone. Obviously, the carbon-budget calculations in IMAGE-2.2 introduce additional uncertainties of a different category, some of which were studied by *Leemans et al.* [2002]. Figure 8 shows that the 70–80 ppmv reduction in CO_2 concentrations in the two mitigation scenarios moderates global-mean temperature increase by about 0.1°C in 2100, thus mitigating global warming over the 21st century by more than 10%.

[41] Although the CO_2 pathways of the two mitigation scenarios IM-C and IM-bio are comparable, the albedo

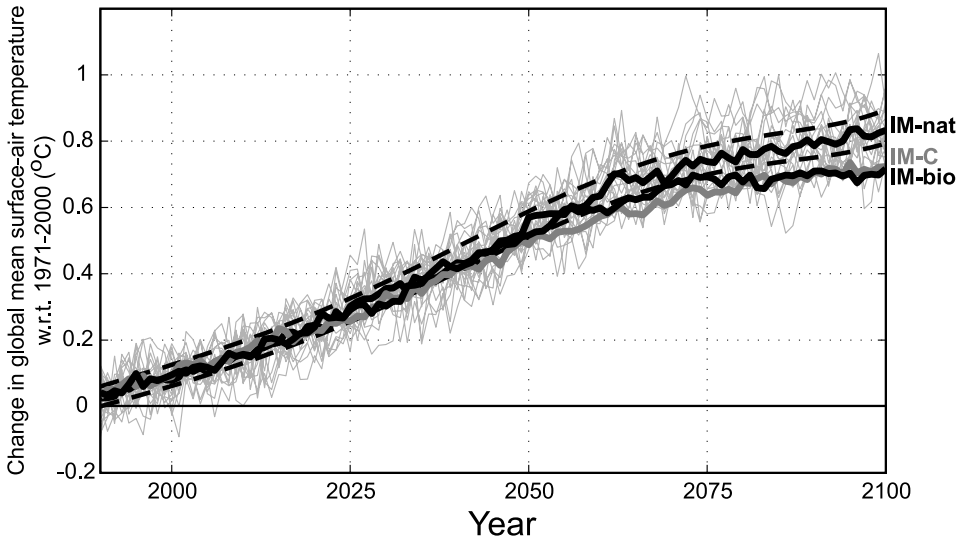

Figure 8. Global and annual mean surface-air temperature in ECBilt-CLIO with respect to 1971–2000 for the CO_2-only experiments, i.e., without taking into account differences in albedo. Thin gray lines are individual ensemble members of the no-plantation baseline experiment. Thick lines are ensemble means of the no-plantation baseline (IM-nat, experiment EC-nat-GHG), C-plantation (IM-C, experiment EC-C-GHG), and MB-plantation (IM-bio, experiment EC-bio-GHG) experiments. The dashed lines indicate the distance to the baseline case beyond which ensemble means differ from the baseline with 95% significance.

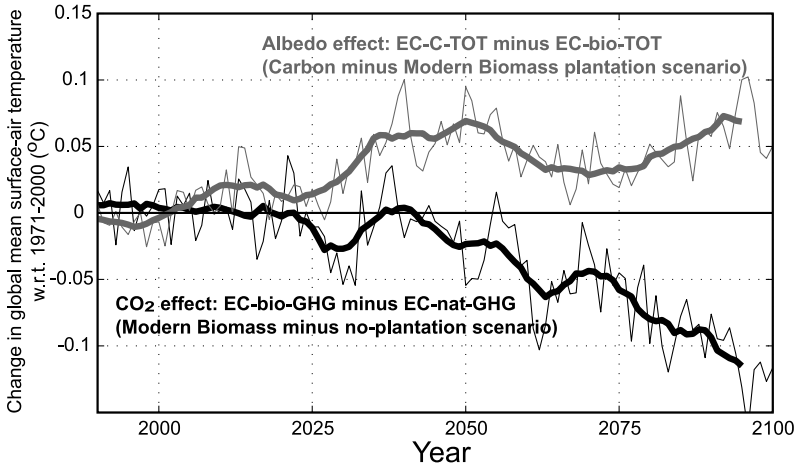

Figure 9. Difference between ensemble averages in global and annual mean surface-air temperature with respect to 1971–2000. The black line indicates the CO_2 effect, i.e., the global cooling resulting only from lower net CO_2 emissions in the two mitigation scenarios (shown for MB-plantation CO_2-only experiment, EC-bio-GHG) compared to the no-plantation baseline (EC-nat-GHG). The red line shows the relative global warming in the C-plantation scenario compared to the MB-plantations scenario, caused by the difference in the pathway of surface albedo (EC-C-TOT minus EC-bio-TOT). Thin lines indicate ensemble mean differences, while thick lines represent the 10-year running mean thereof.

difference causes diverging climate impacts in the EC-C-TOT and EC-bio-TOT experiments (Figure 9, upper line). The global-mean SAT difference between these two experiments increases most rapidly in the first half of the 21st century when large areas of agricultural land are taken out of production in areas with significant snow cover. The low productive agricultural land in these areas is first in line to be selected for abandonment. The global SAT difference after the 2050s stays more or less constant, because additional areas in Russia and China have less snow cover and

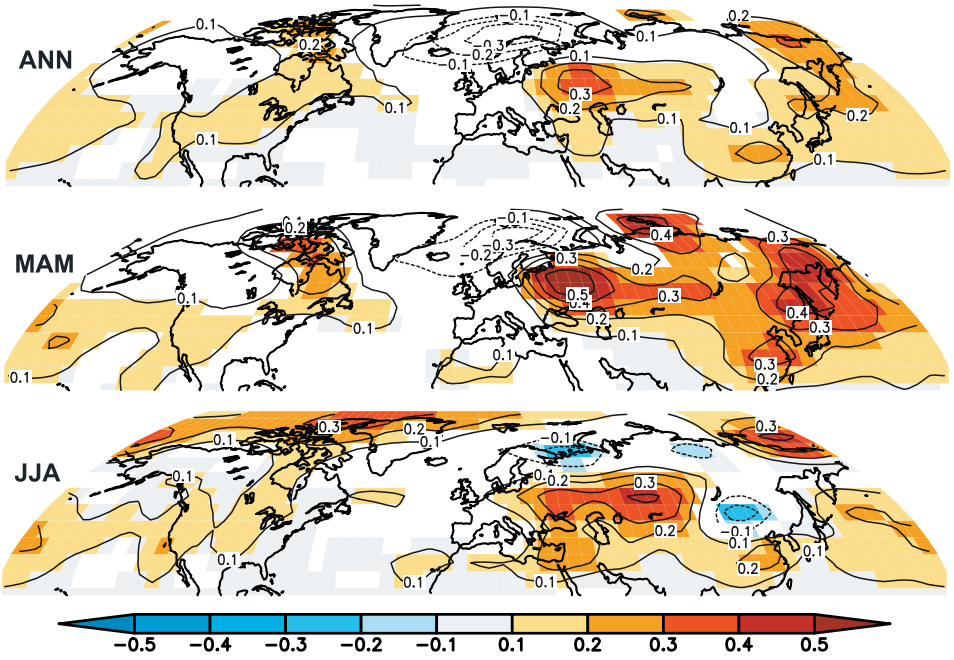

Figure 10. Difference in surface-air temperature in 2071–2100 (°C) including the albedo effects of C-plantation (EC-C-TOT) with respect to MB-plantation (EC-bio-TOT) ensemble (top) for annual mean and averaged over (middle) March-April-May and (bottom) June-July August. Contours are plotted for all model grid cells. Color denotes grid cells for which the difference between the two ensemble means is significant above the 95% level (two-tailed Student's t-test).

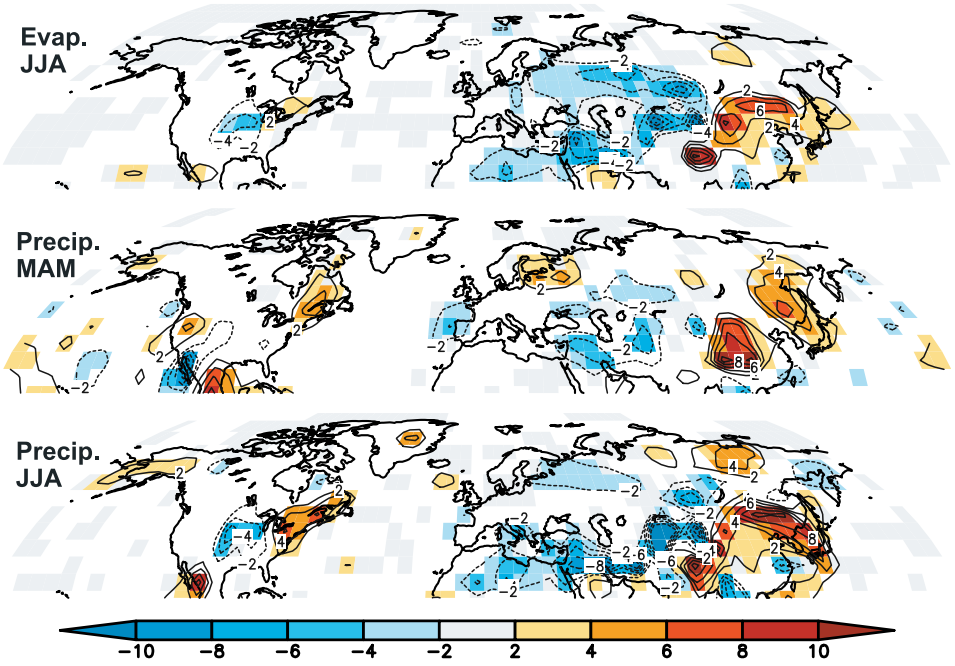

Figure 11. As in Figure 10 for difference in (top) March-April-May and June-July August evaporation, and (middle) March-April-May and (bottom) June-July-August precipitation, all in cm/yr.

because the snow line slowly retreats northward owing to global warming, thus lowering the albedo difference between cropland and forests near the retreating snow line.

[42] In contrast to the albedo impact, it is well after the year 2050 that any significant climate impact can be detected of the gradually reducing CO_2 concentration in the two mitigation options compared to the baseline (Figure 9, lower line). The size of the CO_2 and albedo effects becomes comparable in the last decades of the 21st century model simulation. Thus, although the timing is different, the global climate impact of the albedo difference between the two mitigation scenarios is comparable in size to the impact of the reduced CO_2 concentration in the two mitigation options compared to the baseline.

[43] In the regions of major land-use changes, surface-air temperature is significantly higher in the C-plantation scenario compared to the biomass scenario (compare Figure 10 with Figure 2). The annual mean difference reaches 0.3°C in some regions, which is about 25% of the full local climate change signal over the 21st century in the baseline case. This difference is further up to several times the local temperature difference between the mitigation scenarios and the baseline caused by the 70–80 ppmv difference in CO_2 concentration only. The response in our model is weaker than the response to 21st century afforestation from *Sitch et al.* [2005], who found annual mean warming of 0.1°–0.25°C over North America and 0.25°–0.5°C over Eurasia. The locations of abandoned cropland from *Sitch et al.* [2005], who used the IMAGE-2.2 B1 scenario, are comparable to the locations in the present paper, but the total area was smaller. The weaker response in our case agrees with the generally lower climate sensitivity of our model.

[44] The difference in seasonal-mean temperature response is largest in spring. In this season the patterns of the differences in temperature and albedo strongly resemble each other (Figure 7), suggesting a simple and immediate temperature response to a change in surface shortwave radiative balance.

[45] In contrast, the strong temperature response in summer over central Eurasia is not directly linked to (local) albedo changes. Except for eastern Asia, summer temperatures in Eurasia seem to respond to a reduction in summer evaporative cooling (Figure 11) in areas where the soil moisture buffer is reduced (not shown). Depending on the location, summer soil moisture is reduced by an increase in evaporation in spring or early summer, because of higher temperatures related to a decreased albedo, or by a decrease in spring or summer precipitation (Figure 11). The latter is the case in central Eurasia. In spring, a general weakening of the westerly large-scale circulation is shown for central Eurasia (Figure 12). Thus a warming over northwestern Russia and China in spring seems to weaken the westerly atmospheric supply of moisture in central Eurasia, consequently reducing precipitation. The increase in summer temperature in central Eurasia might also be due to the reduced northerly winds at the northwestern side of the Tibetan plateau.

[46] A second teleconnection is found between land-use changes in Eurasia and precipitation over North Africa, where an annual reduction in precipitation as a percentage of local rainfall reaches 10% (Figure 13). The local increase in northerly wind speed (Figure 12) in the lower troposphere suggests a strengthening of the Hadley cell. The associated

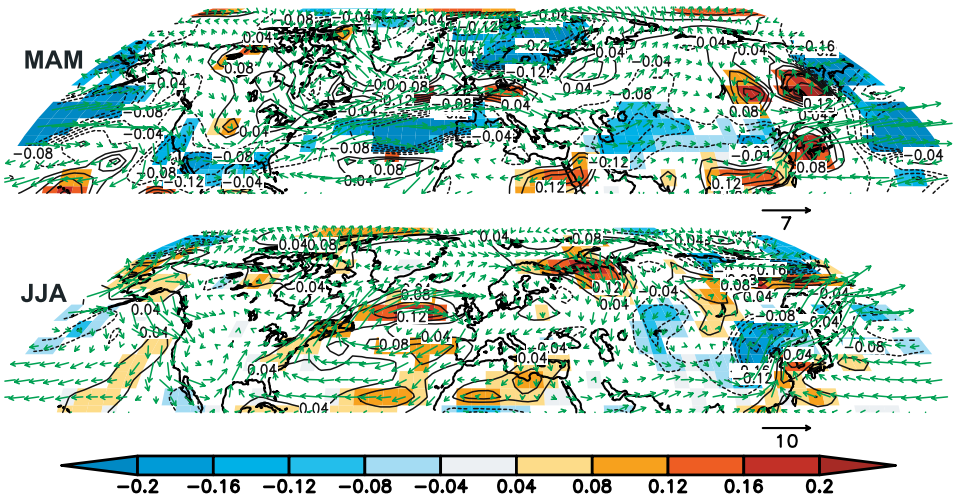

Figure 12. As in Figure 11 for difference in wind speed (m/s) averaged over (top) March-April-May and (bottom) June-July-August. The arrows indicate mean wind direction in the baseline case.

enhancement of downward air motion might explain the simulated reduction in precipitation.

[47] The proposed teleconnections between radiative forcing by albedo changes and remote temperature advection and precipitation indicates that (regional) climate feedbacks complicate the general picture of global warming resulting from decreased surface albedo in the C-plantation scenario compared to MB plantations. Since ECBilt-CLIO is a simplified GCM, one has to take caution in interpreting the results. However, the relatively robust direct local forcing by albedo changes implies that other climate effects than just the impact of changes in CO_2 concentrations need to be taken into account when assessing mitigation options that involve land-use changes. The complex picture that emerges from the teleconnections mentioned above emphasizes this conclusion.

8. Discussion and Conclusions

[48] Our analysis shows that the large-scale application of carbon and modern-biomass plantations in the northern extra-tropics causes changes in surface-albedo and CO_2 concentration. The lower albedo of carbon plantations results in significantly higher regional and global-mean surface-air temperatures than in the modern-biomass-plantation scenario. The impact on CO_2 concentrations of these two mitigation options is comparable.

[49] The changes in climate due to albedo changes accelerate rapidly on the short-to-medium term, while the CO_2 concentrations gradually increase up to the end of the 21st century. By that time, the CO_2 effect on climate has become somewhat larger than that of albedo change. Albedo change thus gradually becomes less important relative to the impact of changes in CO_2, but is the dominant forcing in these scenarios over the larger part of the 21st century. Carbon plantations are often brought forward as an option to "buy time" for the medium term, allowing a longer delay of transformations in the energy sector. Since we found that on the short-to-medium term the albedo effect is strongly unfavorable for the carbon-plantations case, it is questionable whether carbon plantations in the Northern Hemisphere could actually fulfill such an effective role in medium-term mitigation efforts. On the centennial timescale, over which the albedo effect becomes relatively less important, the permanency of carbon plantations is questionable [e.g., *Barford et al.*, 2001].

[50] The IPCC A1b land-use scenario, which forms the basis for our sensitivity experiments, is subject to some uncertainty that is typical of geographical patterns of climate change. We have used IMAGE 2.2 earlier with climate change patterns from a variety of Coupled Global Circulation Models (CGCMs) [*IMAGE-team*, 2001b]. The principle conclusion is that even at the end of the 21st century the sensitivity of land-cover changes to climate-

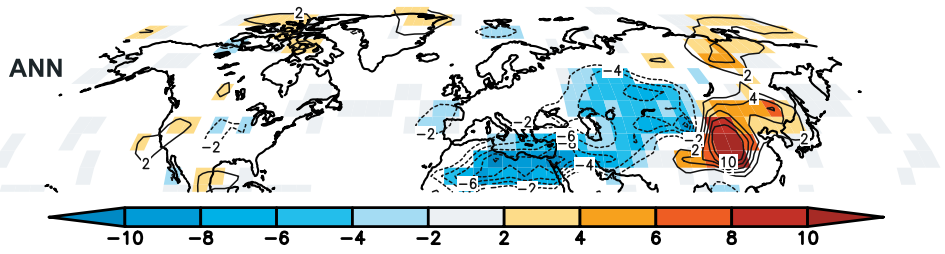

Figure 13. As in Figure 11 for relative difference in annual mean precipitation (%).

change patterns is low on the spatial scale of IMAGE-2.2 regions (subcontinental scale) and the uncertainty is largely driven by socio-economics. Moreover, the difference is necessarily much smaller between the baseline and the two mitigation scenarios, because the difference in CO_2 concentration is "only" 70–80 ppmv; thus the difference between climate change patterns of different CGCMs is also smaller. A remaining issue forms a basic shortcoming in an exercise using a chain of models. In our analyses a feedback of albedo-induced climate change in the climate model to the land-cover model is absent. For example, the relative regional warming in the carbon-plantation scenario by albedo differences might impact on CO_2 uptake and thus the global CO_2 concentration. However, we consider this of secondary importance.

[51] The climate sensitivity of our climate model is on the lower side of the range spanned by CGCMs [*IPCC*, 2001; *Raper et al.*, 2002], as well as the range found plausible in dedicated climate-sensitivity estimates [*Andronova and Schlesinger*, 2001; *Forest et al.*, 2002; *Harvey and Kaufmann*, 2002; *Knutti et al.*, 2002]. This is an important aspect to consider, since we are concerned with the relative impact of changes in greenhouse-gas concentration and land-surface albedo and these two drivers act on climate through different mechanisms. *Drijfhout et al.* [1999] argue that an earlier, but on essential points comparable, version of ECBilt was in general a relatively insensitive climate model. Not only was the climate sensitivity roughly half of the mean of CGCMs, the amplitude of midlatitude (internal) climate variability and the response to a change in (external) solar forcing was also about half of that found in CGCMs. The relative contribution of these components to the total climate variations was, however, comparable. Recently, we have compared the response of ECBilt with five other Earth System Models of Intermediate Complexity (EMICs) to a time series of historical (1700–2000) land-use changes [*Brovkin et al.*, 2006]. Compared to these models, the response of ECBilt to land-cover changes is on the lower side of the mean in terms of global-mean temperature, as was its response to CO_2 increase. This comparison is confirmed by the stronger temperature response from *Sitch et al.* [2005] to both a milder afforestation scenario in comparable regions and a comparable increase in CO_2. These considerations lead us to believe that the relative impact of the changes in greenhouse-gas concentrations and land-surface albedo that we presented here is reasonably robust.

[52] In this paper we have concentrated on the albedo impact of land-use changes, because this is the main driver of land-use related climate change in the extra-tropics. However, the processes are more complex in the tropics (see *Pielke* [2001b] for an interesting overview). Here the hydrological cycle plays a dominant role and albedo differences are not the single most important driver [*Niyogi et al.*, 2002; *Kabat et al.*, 2004]. In addition, teleconnections between the tropics and the extratropics give rise to a complex picture of land-use changes in the tropics causing changes in climate over large distances [*Avissar*, 1995]. Our current analysis explicitly excluded the tropics because the climate model that we used is not viable for assessing the climate impacts of land-use changes in the tropics. One can argue that in the tropics the relative importance of the biophysical climate impacts of land-use changes might be much lower compared to CO_2 changes, since plantations are potentially much more productive in the tropics (van Minnen et al., manuscript in preparation, 2006). Thus our main conclusion that biophysical climate impacts are highly unfavorable to carbon plantations does probably not apply to the tropics.

[53] Although extratropical changes in albedo drive the climate changes in our comparison between the two mitigation scenarios, it seems that a major response of temperature change in summer can only be explained by a modification of large-scale circulation, which causes changes in the hydrological cycle, including a remote response in central Eurasia and North Africa. The projected temperature changes in central Eurasia and precipitation changes in North Africa are sizable. Because the mechanisms are less transparent than a simple direct warming by lowered albedo, they deserve careful study with state-of-the-art, higher-resolution CGCMs. This could help to gain a more complete understanding of the full climate effect of plantation mitigation options. The current discussions of such mitigation options in the policy context of the UNFCCC mean that such research is urgent.

Appendix A

[54] For the calculation of grid-cell albedo (snow and snow-free) in the ECBilt-CLIO climate model, parameter values were derived from a variety of sources. When available, values were adopted from field studies. If these were not available, or ambiguous, the parameter values were found by optimizing the correlation between satellite albedo and modeled albedo, using present-day land-cover

Table A1. Snow-Free (α) and Fresh-Snow-Covered (α_{fresh}) Albedo Values for ECBilt Vegetation Types[a]

Land-Cover Type	Ref	α	α_{fresh}
Crops	1,5,sat	0.19	0.75
Biomass energy crops	1,5	0.18	0.70
Polar desert	sat	0.80	0.80
Polar desert2 (Greenland ice sheet)	sat	0.84	0.84
Polar desert3 (Antarctic ice sheet)	sat	0.87	0.87
Sand desert (Sahara)	sat	0.34	-
Sand desert (semi desert)	sat	0.27	0.7
Arctic grasses and shrubs	4	0.15	0.8
Grasses C3	1,5,6,7,8	0.19	0.65
Grasses C4	1,7,8	0.21	0.6
Deciduous shrubs	1	0.18	0.6
Evergreen shrubs	1	0.18	0.5
Deciduous needleleaf trees	1,2,5	0.12	0.3
Evergreen needleleaf trees	1,2,4,5	0.11	0.2
Deciduous broadleaf trees	1,2	0.13	0.3
Evergreen broadleaf trees	8	0.13	0.2
Tropical deciduous broadleaf trees	1	0.13	-

[a]The Ref column lists the references to near-ground measurements: 1, *Robinson and Kukla* [1984]; 2, *Robinson and Kukla* [1985]; 3, *Harding and Pomeroy* [1996]; 4, *Eck et al.* [1997]; 5, *Sharrat* [1998]; 6, *Douville and Royer* [1997]; 7, *Fennessy and Xue* [1997]; 8, *O'Brien* [1996]. Albedos adjusted or defined after comparison of ECBilt surface albedo (using the 1990 IMAGE-2.2 land-cover map) with satellite data [*Barkstrom*, 1984] are indicated by "sat".

Table A2. Fractional Coverage of ECBilt Vegetation Types in IMAGE-2.2 Land-Cover Classes

	ECBilt Type												
IMAGE Type	Crops	Biomass Energy Crops	Polar Desert	Sand Desert	Arctic Grasses and Herbs	Grasses C3	Grasses C4	Deciduous Shrubs	Evergreen Shrubs	Deciduous Needleleaf Trees	Evergreen Needleleaf Trees	Deciduous Broadleaf Trees	Evergreen Broadleaf Trees	Tropical Deciduous Broadleaf Trees
Agricultural land	1.00													
modern biomass plantation		1.00												
broadleaf C plantation						0.05		0.05				0.90		
needleleaf C plantation						0.05		0.05			0.90			
polar desert			1.00											
hot desert				1.00										
Tundra					0.80			0.20						
wooded tundra					0.45			0.30	0.10		0.15			
boreal forest					0.25			0.05	0.05	0.10	0.45	0.10		
cool conifer forest					0.05	0.05		0.05	0.10	0.10	0.50	0.15		
temperate mixed forest						0.10		0.10	0.05		0.35	0.40		
temperate deciduous forest						0.10		0.10				0.80		
warm mixed forest						0.10	0.10				0.40	0.20	0.20	
cool grassland						1.00								
warm grassland						0.80	0.20							
C4 grassland						0.20	0.80							
Scrubland						0.20	0.20	0.60						0.25
Savanna						0.10	0.40	0.25					0.10	0.40
tropical woodland							0.10	0.20	0.20				0.80	0.20
tropical forest														

maps of IMAGE-2.2 and snow-cover maps from present-day simulation of ECBilt-CLIO. In Tables A1 and A2 the parameter values are given as used in the model experiments, with reference to the (literature) source.

References

Alcamo, J., R. Leemans, and E. E. Kreileman (1998), *Global Change Scenarios in the 21st Century: Results From the IMAGE 2.1 Model*, Elsevier, New York.

Andronova, N., and M. E. Schlesinger (2001), Objective estimation of the probability distribution for climate sensitivity, *J. Geophys. Res.*, *106*, 22,605–22,612.

Avissar, R. (1995), Recent advances in the representation of land-atmosphere interactions in general circulation models, *Rev. Geophys.*, *33*, 1005–1010.

Barford, C. C., S. C. Wofsy, M. L. Goulden, J. W. Munger, E. H. Pyle, S. P. Urbanski, L. Hutyra, S. R. Saleska, D. Fitzjarrald, and K. Moore (2001), Factors controlling long- and short-term sequestration of atmospheric CO_2 in a mid-latitude forest, *Science*, *294*, 1688–1691.

Barkstrom, B. R. (1984), The Earth Radiation Budget Experiment (ERBE), *Bull. Am. Meteorol. Soc.*, *65*, 1170–1185.

Berndes, G., M. Hoogwijk, and R. van den Broek (2003), The contribution of biomass in the future global energy supply: A review of 17 studies, *Biomass Bioenergy*, *25*, 1–28.

Betts, R. A. (2000), Offset of the potential carbon sink from boreal forestation by decreases in surface albedo, *Nature*, *408*, 187–190.

Bonan, G. B., F. S. Chapin III, and S. L. Thompson (1995), Boreal forest and tundra ecosystems as components of the climate system, *Clim. Change*, *29*, 145–167.

Brovkin, V., A. Ganopolski, M. Claussen, C. Kubatzki, and V. Petukhov (1999), Modelling climate response to historical land cover change, *Global Ecol. Biogeogr.*, *8*, 509–517.

Brovkin, V., M. Claussen, E. Driesschaert, T. Fichefet, D. Kicklighter, M.-F. Loutre, H. D. Matthews, N. Ramankutty, M. Schaeffer, and A. Sokolov (2006), Biogeophysical effects of historical land cover changes simulated by six Earth system models of intermediate complexity, *Clim. Dyn.*, *26*, 587–600.

Chase, T. N., R. A. Pielke Sr., T. G. F. Kittel, R. R. Nemani, and S. W. Running (2000), Simulated impacts of historical land cover changes on global climate in northern winter, *Clim. Dyn.*, *16*, 93–105.

Cox, P. M., R. A. Betts, C. B. Bunton, R. L. H. Essery, P. R. Rowntree, and J. Smith (1999), The impact of new land surface physics on the GCM simulation of climate and climate sensitivity, *Clim. Dyn.*, *15*, 183–203.

Cramer, W., and A. M. Solomon (1993), Climate classification and future global redistribution of agricultural land, *Clim. Res.*, *3*(1–2), 97–110.

de Vries, H. J. M., D. P. van Vuuren, M. G. J. den Elzen, and M. A. Janssen (2001), The TARGETS IMage Energy Regional (TIMER) model, *Rep. 461502024/2001*, Natl. Inst. for Public Health and the Environ. (RIVM), Bilthoven, Netherlands.

Douville, H., and J.-F. Royer (1997), Influence of the temperate and boreal forests on the Northern Hemisphere climate in the Météo-France climate model, *Clim. Dyn.*, *13*, 57–74.

Drijfhout, S. S., R. J. Haarsma, J. D. Opsteegh, and F. M. Selten (1999), Solar-induced versus internal climate variability in a coupled climate model, *Geophys. Res. Lett.*, *26*, 205–208.

Eck, T. F., D. W. Deering, and L. A. Vierling (1997), Arctic tundra albedo and its estimation from spectral hemispheric reflectance, *Int. J. Remote Sens.*, *18*, 3535–3549.

Eickhout, B., M. G. J. den Elzen, and G. J. J. Kreileman (2004), The Atmosphere-Ocean System of IMAGE 2.2: A global model approach for atmospheric concentrations, and climate and sea level projections, report, Natl. Inst. for Public Health and the Environ. (RIVM), Bilthoven, Netherlands.

Fennessy, M. J., and Y. Xue (1997), Impact of USGS vegetation map on GCM simulations over the United States, *Ecol. Appl.*, *7*, 22–33.

Forest, C. E., P. H. Stone, A. P. Sokolov, M. R. Allen, and M. Webster (2002), Quantifying uncertainties in climate system properties with the use of recent climate observations, *Science*, *295*, 113–117.

Foster, D. J., and R. D. Davy (1988), Global snow depth climatology, *Rep. USAFETAC/TN-88/006*, Scott Air Force Base, Ill.

Goosse, H., and T. Fichefet (1999), Importance of ice-ocean interactions for the global ocean circulation: A model study, *J. Geophys. Res.*, *104*, 23,337–23,355.

Goosse, H., F. M. Selten, R. J. Haarsma, and J. D. Opsteegh (2001), Decadal variability in high Northern latitudes as simulated by an intermediate-complexity climate model, *Ann. Glaciol.*, *33*, 525–532.

Goosse, H., F. M. Selten, R. J. Haarsma, and J. D. Opsteegh (2002), A mechanism of decadal variability of the sea-ice volume in the Northern Hemisphere, *Clim. Dyn.*, *19*, 61–83.

Gregory, J. M., R. J. Stouffer, S. C. B. Raper, P. A. Stott, and N. A. Rayner (2002), An observationally based estimate of the climate sensitivity, *J. Clim.*, *15*, 3117–3121.

Hansen, J., G. Russell, D. Rind, P. Stone, A. Lacis, S. Lebedeff, R. Ruedy, and L. Travis (1983), Efficient three-dimensional global models for climate studies: Models I and II, *Mon. Weather Rev.*, *111*, 609–662.

Harding, R. J., and J. W. Pomeroy (1996), The energy balance of the winter boreal landscape, *J. Clim.*, *9*, 2778–2787.

Harvey, L. D. D., and R. K. Kaufmann (2002), Simultaneously constraining climate sensitivity and aerosol radiative forcing, *J. Clim.*, *15*, 2837–2861.

Hoogwijk, M., A. Faaij, B. Eickhout, B. de Vries, and W. Turkenburg (2005), Potential of biomass energy out to 2100, for four IPCC SRES land-use scenarios, *Biomass Bioenergy*, *29*, 225–257.

IMAGE-team (2001a), *The IMAGE 2.2 Implementation of the SRES Scenarios: A Comprehensive Analysis of Emissions, Climate Change and Impacts in the 21st Century* [CD-ROM], Natl. Inst. for Public Health and the Environ. (RIVM), Bilthoven, Netherlands.

IMAGE-team (2001b), The IMAGE 2.2 Implementation of the SRES Scenarios. Climate Change Scenarios Resulting From Runs With Several GCMs [CD-ROM] Natl. Inst. for Public Health and the Environ. (RIVM), Bilthoven, Netherlands.

Intergovernmental Panel on Climate Change (2000), *Emissions Scenarios: A Special Report of Working Group III of the Intergovernmental Panel on Climate Change*, Cambridge Univ. Press, New York.

Intergovernmental Panel on Climate Change (2001), *Climate Change 2001—The Scientific Basis: Contribution of Working Group I to the Third Assessment Report of the Intergovernmental Panel on Climate Change*, Cambridge Univ. Press, New York.

Kabat, P., M. Claussen, P. A. Dirmeyer, J. H. C. Gash, L. B. de Guenni, M. Meybeck, R. A. Pielke Sr., C. J. Vörösmarty, R. W. A. Hutjes, and S. Lütkemeier (2004), *Vegetation, Water, Humans and the Climate. A New Perspective on an Interactive System*, Springer, New York.

Kattenberg, A., F. Giorgi, H. Grassl, G. A. Meehl, J. F. B. Mitchell, R. J. Stouffer, T. Tokioka, A. J. Weaver, and T. M. L. Wigley (1996), Climate models: Projections of future climate, in Climate change 1995: The science of Climate change. Contribution of Working Group I to the Second Assessment Report of the International Panel on Climate Change, edited by J. T. Houghton et al., pp. 285–358, Cambridge Univ. Press, New York.

Knutti, R., T. F. Stocker, F. Joos, and G.-K. Plattner (2002), Constraints on radiative forcing and future climate change from observations and climate model ensembles, *Nature*, *416*, 719–723.

Leemans, L., and G.-J. van den Born (1994), Determining the potential global distribution of natural vegetation, crops and agricultural productivity, *Water Air Soil Pollut.*, *76*, 133–161.

Leemans, R., B. Eickhout, B. Strengers, L. Bouwman, and M. Schaeffer (2002), The consequences of uncertainties in land use, climate and vegetation responses on the terrestrial carbon, *Sci. China*, *45*, 126–142.

Marland, G., et al. (2003), The climatic impacts of land surface change and carbon management, and the implications for climate-change mitigation policy, *Clim. Policy*, *3*, 149–157.

Nabuurs, G. J., and G. M. J. Mohren (1996), Modelling analysis of potential carbon sequestration in selected forest types, *Can. J. For. Res.*, *25*, 1157–1172.

Niyogi, D. S., Y.-K. Xue, and S. Raman (2002), Hydrological feedback in a land-atmosphere coupling: Comparison of a tropical and a midlatitudinal regime, *J. Hydrometeorol.*, *3*, 39–56.

O'Brien, K. L. (1996), Tropical deforestation and climate change, *Prog. Phys. Geogr.*, *20*, 311–335.

Opsteegh, J. D., R. J. Haarsma, F. M. Selten, and A. Kattenberg (1998), ECBILT: A dynamic alternative to mixed boundary conditions in ocean models, *Tellus, Ser. A*, *50*, 348–367.

Pielke, R. A., Sr. (2001a), Carbon sequestration: The need for an integrated climate system approach, *Bull. Am. Meteorol. Soc.*, *82*, 2021–2022.

Pielke, R. A., Sr. (2001b), Influence of the spatial distribution of vegetation and soils on the prediction of cumulus convective rainfall, *Rev. Geophys.*, *39*, 151–177.

Pielke, R. A., Sr., G. Marland, R. A. Betts, T. N. Chase, J. L. Eastman, J. O. Niles, D. D. S. Niyogi, and S. W. Running (2002), The influence of land-use change and landscape dynamics on the climate system: Relevance to climate-change policy beyond the radiative effect of greenhouse gases, *Philos. Trans. R. Soc.*, *360*, 1705–1719.

Prentice, I. C., W. Cramer, S. P. Harrison, R. Leemans, R. A. Monserud, and A. M. Solomon (1992), A global biome model based on plant physiology and dominance, soil properties and climate, *J. Biogeogr.*, *19*, 117–134.

Raper, S. C. B., J. M. Gregory, and R. J. Stouffer (2002), The role of climate sensitivity and ocean heat uptake on AOGCM transient temperature response, *J. Clim.*, *15*, 124–130.

Renssen, H., H. Goosse, T. Fichefet, and J.-M. Campin (2001), The 8. 2 kyr BP event simulated by a global atmosphere-sea-ice-ocean model, *Geophys. Res. Lett.*, *28*, 1567–1570.

Robinson, D. A., and G. Kukla (1984), Albedo of a dissipating snow cover, *J. Clim. Appl. Meteorol.*, *23*, 1626–1634.

Robinson, D. A., and G. Kukla (1985), Maximum surface albedo of seasonally snow-covered lands in the Northern Hemisphere, *J. Clim. Appl. Meteorol.*, *24*, 402–411.

Schaeffer, M., F. M. Selten, J. D. Opsteegh, and H. Goosse (2002), Intrinsic limits to predictability of abrupt regional climate change in IPCC SRES scenarios, *Geophys. Res. Lett.*, *29*(16), 1767, doi:10.1029/2002GL015254.

Schaeffer, M., F. M. Selten, J. D. Opsteegh, and H. Goosse (2004), The influence of ocean convection patterns on high-latitude climate projections, *J. Clim.*, *17*, 4316–4329.

Schaeffer, M., F. M. Selten, and J. D. Opsteegh (2005), Shifts of means are not a proxy for changes in extreme winter temperatures in climate projections, *Clim. Dyn.*, *25*(1), 51–63.

Sharrat, B. S. (1998), Radiative exchange, near-surface temperature and soil water of forest and cropland in interior Alaska, *Agric. For. Meteorol.*, *89*, 269–280.

Sitch, S., V. Brovkin, W. von Bloh, D. Van Vuuren, B. Eickhout, and A. Ganopolski (2005), Impacts of future land cover on atmospheric CO_2 and climate, *Global Biogeochem. Cycles*, *19*, GB2013, doi:10.1029/2004GB002311.

Strengers, B., R. Leemans, B. J. Eickhout, H. J. M. de Vries, and A. F. Bouwman (2004), The land use projections in the IPCC SRES scenarios as simulated by the IMAGE 2.2 model, *Geojournal*, *61*, 381–393.

Strengers, B., J. G. van Minnen, and B. J. Eickhout (2005), The role of carbon plantations in mitigating climate change: Potentials and costs, report, Neth. Environ. Assess. Agency, Natl. Inst. for Public Health and the Environ. (RIVM), Bilthoven, Netherlands.

van Vuuren, D. P., B. Eickhout, P. L. Lucas, and M. G. J. den Elzen (2006), Long-term multi-gas scenarios to stabilise radiative forcing–Exploring costs and benefits within an integrated assessment framework, *Energy Policy*, in press.

B. Eickhout, B. Strengers, and D. van Vuuren, Global Sustainability and Climate, Netherlands Environmental Assessment Agency (MNP), PO Box 303, NL-3720 AH Bilthoven, Netherlands. (bas.eickhout@mnp.nl; bart.strengers@mnp.nl; detlef.van.vuuren@mnp.nl)

M. Hoogwijk, Ecofys B.V., P.O. Box 8408, NL-3503 RK Utrecht, Netherlands. (m.hoogwijk@ecofys.nl)

R. Leemans, Environmental Systems Analysis Group, Wageningen University and Research (WUR), PO Box 47, NL-6700 AA Wageningen, Netherlands. (rik.leemans@wur.nl)

T. Opsteegh, Institute for Marine and Atmospheric Research Utrecht (IMAU), Faculty of Physics and Astronomy, Utrecht University, PO Box 80000, NL-3508 TA Utrecht, Netherlands. (j.d.opsteegh@phys.uu.nl)

M. Schaeffer (corresponding author), Environmental Systems Analysis Group, Wageningen University and Research Centre (WUR), Bode 145, P.O. Box 8080, NL-6700 DD Wageningen, Netherlands. (Michael.Schaeffer@wur.nl)